

Forced Convection Heat Transfer of Drag Reducing Fluid Flow In A Cylindrical Porous Medium

انتقال الحرارة بالحمل الجبري للموائع المخفضة للجر الاحتكاكي في وسط مسامي اسطواني

M.S. El-Kady and L.H. Rabie

Mechanical Power Engineering Department
Mansoura University, Egypt

خلاصه:

في هذا البحث أجريت دراسة عديدة لانتقال الحرارة بالحمل الجبري من سريان الموائع اللانيوتونية (المخفضة للجر الاحتكاكي) في مجرى اسطواني مملوء بوسط مسامي كروي مشبع ذو حائط معرض اما لفيض حراري ثابت أو درجة حرارة ثابتة، تم فيها دراسة تأثير اللزوجة الطولية للموائع اللانيوتونية المخفضة للجر الاحتكاكي على خواص انتقال الحرارة. تكون النموذج العددي من معادلة الطاقة بالإضافة الى معادلة كمية الحركة المعدلة (دارسي-فورشمهايمر-برينكمان) والتي تم فيها الأخذ في الاعتبار لكل من التأثيرات اللادارسية المختلفة مثل المسامية المتغيرة، للتصور الذاتي والاحتكاك اللزج عند الحوائط لبرينكمان وذلك بالإضافة الى تأثير اللزوجة الطولية اللانيوتونية للمائع وتم حله باستخدام طريقة النروق البسيطة. أجريت الدراسة النظرية لسريان ذو معامل احتكاك لانيوتوني بمدى $0 \leq \psi \leq 5000$ ومعامل احدار الضغط B يصل الى 10^8 . وأظهرت النتائج أن التأثيرات اللانيوتونية لها تأثيرا واضحا على كل من طول المدخل الحراري ومعامل انتقال الحرارة المتمثل في عدد نوسيلت وكذلك على شكل توزيع درجات الحرارة في مقطع المجري، وان سوائل ذات معامل احتكاك لانيوتوني منخفض جدا يمكن أن تسبب نقصا كبيرا في طول المدخل الحراري وزيادة كبيرة في عدد نوسيلت في المنطقة كاملة التطور وكذلك نقصان كبير في فرق درجات الحرارة بين الحائط وقلب الوسط المسامي وانتشار أسرع لحرارة السطح الى المنطقة الداخلية، وتعطى نتائج هذه الدراسة تحليلا لسلوك كل من طول المدخل الحراري وعدد نوسيلت وتوزيع درجات الحرارة واعتمادهما على معامل الاحتكاك اللانيوتوني. وتم حل المعادلات تحت حالات مناظرة لحالات بوليكاكوس وريبنكن [20] ومقارنة عدد نوسيلت في المنطقة كاملة التطور بنتائج هذا النموذج. أظهرت المقارنة تطابقا جيدا للنتائج وصحة هذا النموذج.

Abstract:

The present analysis investigates non-Darcy forced convective heat transfer in a cylindrical pipe filled with spherical beads saturated with non-Newtonian drag reducing fluid. The cylindrical pipe is subjected to either a uniform heat flux (UHF) or a constant wall temperature (CWT). In modeling the flow, both the energy equation and a modified momentum (Darcy-Forschheimer-Brinkman) equation are used, in which the variable porosity, flow inertia, Brinkman viscous friction (non-Darcian effects) besides the elongational viscosity of drag reducing fluids are taken into consideration and the finite difference technique is used. The results are obtained for a non-Newtonian drag parameter range of $0 \leq \psi \leq 5000$, and nondimensional pressure gradient B up to 10^8 . The results show that the non-Newtonian character of drag reducing fluids have a significant influence on the entrance length, heat transfer characteristics and the temperature profiles. Important results documenting and analyzing the behavior of the entrance length and the

heat characteristics and its dependence on the non-Newtonian drag parameter are also reported. To examine the adequacy of the present heat transfer model, the governing equations were solved under conditions corresponding to those in Poulikakos and Renken [20]. The comparison of the calculated Nu_f with that of Poulikakos and Renken [20] for $d=3$ and 5 mm, $\psi = 0$, $0.05 \leq D \leq 0.15$ and $10^4 \leq B \leq 10^6$ shows good agreement and validates the presented heat transfer model.

1. Introduction

In the area of convection heat transfer in porous media, the bulk of the literature is directed towards the understanding of heat transfer to only Newtonian fluids. Even the comprehensive review articles of Shenoy [1,2] which essentially discuss heat transfer to non-Newtonian fluids show that at least until then there were no heat transfer studies considering non-Newtonian fluid-saturated porous media. However, the status is quite different now with large number of research papers having been published on heat transfer in non-Newtonian fluid saturated porous medium [3-14]. This is because of the envisaged importance of understanding changes in heat transfer with non-Newtonian flow behavior in the area of ceramic processing, enhanced oil recovery, polymer processing, chemical industries and filtration.

Chen and Chen [3] were the first to consider the simplest steady state free convection flow of non-Newtonian power law fluids past an isothermal vertical flat plate embedded in a porous medium. Forced- and natural convection boundary layer flow and heat transfer of a Herschel-Bulkley-type non-Newtonian fluid past an isothermal semi-infinite plate in porous media was analytically explored by Wang and Tu [4]. Pascal and Pascal [5] considered constant temperature and constant flux boundary layer flow of a Herschel-Bulkley fluid along a heated vertical cylinder. The unsteady state solution of the case of a shear thinning fluid in the presence of a yield stress was obtained by Pascal [6]. Wang et al. [7] investigated the mixed convection of non-Newtonian fluids from a vertical isothermal plate embedded in a homogeneous porous medium. Buoyancy-induced flow of non-Newtonian fluids over a non-isothermal body of arbitrary shape in a fluid saturated porous medium was treated by Nakayama and Koyama [8]. Combined free-and forced convection heat transfer to power law fluid-saturated porous media was analyzed by Nakayama and Shenoy [9] and similarity solutions were presented for vertical flat plates, cones, horizontal cylinders and spheres. Amiri et al. [10] studied analytically and numerically the buoyancy induced flows of power law fluids in a horizontally fluid saturated porous layer subjected to constant heat flux. Yang and Wang [11] analyzed the natural convection of a non-Newtonian power-law fluid with or without yield stress about a two-dimensional or axisymmetric body of arbitrary shape in a fluid saturated porous medium.

All the above mentioned non-Newtonian fluid saturated porous media studies deal with only Darcy flow model. However, it is well known that the Darcy flow model (which assumes proportionality between the velocity and pressure gradient) breaks down when the inertia resistance becomes comparable with the viscous resistance. For Newtonian fluids, Forschheimer proposed a square velocity term in addition to the

Darcian velocity term to account for the inertia resistance effect. The modified form of the Darcy-Forschheimer equation for non-Newtonian power law fluids has been developed recently by Shenoy [12]. Using the proposed equation for mathematically describing non-Darcy flows, the problem of steady state Darcy-Forschheimer natural, forced, and mixed convection for non-Newtonian power law fluid-saturated porous medium has been studied comprehensively by Shenoy [12] for the isothermal flat plate. Nakayama and Shenoy [13] proposed a uniform transformation from which all possible similarity solutions could be deduced for Darcy and Forschheimer convective flow of power law fluids.

None of the studies mentioned above have treated porous media with high permeability, wherein the viscous effects become important due to the frictional drag. Vafsa and Kim [15] comments that the Brinkman-Forschheimer-extended Darcy formulation, if not perfect, is the most commonly used equation in this regard. This accounts for the boundary layer development and macroscopic shear stress, as well as microscopic shear stress and microscopic inertial force. For Newtonian fluid saturated porous media, studies which include the Brinkman term are those of [16-20] for confined flows and those of [21-22] for external flows. For non-Newtonian fluid saturated porous media, Nakayama and Shenoy [14] reported that such non-Darcian flow studies which take into consideration both the Forschheimer inertial, and the Brinkman viscous terms were absent. In Nakayama and Shenoy work [14], the Brinkman-Forschheimer extended Darcy model is used for studying the flow confined within parallel walls subjected to uniform heat flux and immersed in a porous medium saturated with a non-Newtonian power-law fluid.

The above relatively little studies for non-Newtonian fluid saturated porous media were concerned with the power law and Herschel-Bulkley-type non-Newtonian fluids. The flow of the drag reducing type non-Newtonian fluid saturated porous media is not considered. The convective flow through confined channel specially in cylindrical channel is absent. The effect of porosity variation near the wall was not taken into consideration.

The modified form of Brinkman-Forschheimer extended Darcy model for the non-Newtonian drag reducing fluids has been developed recently by El-Kady et al. [23]. In the present work, the proposed model with the variable porosity near the wall is considered. A detailed numerical analysis of forced convection through a cylindrical pipe filled with spherical beads exposed to constant wall temperature (CWT) and uniform heat flux (UHF) is studied. The effect of non-Newtonian drag reducing character on thermal entrance length, temperature variation and heat flow characteristics have been comprehensively discussed.

2. Mathematical Formulation

The physical model considered is a horizontal cylindrical pipe filled with porous medium and is subjected to either uniform heat flux q_w on the outer surface or isothermal wall of temperature T_w as shown in Fig. 1. The porous medium is a packed bed consisting of packed spheres. It is assumed that the fluid and the solid matrix are in local thermal equilibrium. The thermophysical properties of the solid matrix and fluid are

assumed to be constant. The problem has been studied assuming that the flow is steady, incompressible, and hydrodynamically fully developed. The buoyancy force, pressure work and viscous dissipation are neglected. Under these assumptions, the energy equation can be written as:

$$u \frac{\partial T}{\partial x} = \alpha_e \cdot \frac{1}{r} \cdot \frac{\partial}{\partial r} (r \frac{\partial T}{\partial r}) \quad (1)$$

where u , T , α_e are velocity in the axial direction x , Temperature and effective thermal diffusivity.

A modified form of x -momentum (Darcy-Forschheimer-Brinkman) equation for the flow of non-Newtonian drag reducing fluids in a porous medium in cylindrical coordinates is derived by El Kady et al. [23] as;

$$\frac{1}{\rho} \cdot \left[\frac{\partial P}{\partial x} \right] = \frac{\nu}{r} \left[\frac{\partial}{\partial r} (r \frac{\partial u}{\partial r}) \right] - \frac{\nu u}{\gamma} - A u^2 - \frac{\nu u}{\beta} \quad (2)$$

where, ρ , ν are the fluid density and dynamic viscosity respectively. γ and A are the permeability and the inertia coefficient (Forschheimer function) of the porous medium, which are dependent on the porosity " ϵ " and other geometrical parameters of the medium. These parameters are given by Ergun [25] for packed beds of identical spherical particles of diameter " d " and porosity " ϵ " as:

$$\gamma = \frac{d^2 \epsilon^3}{175 (1 - \epsilon)^2}, \quad A = \frac{175 (1 - \epsilon)}{d \epsilon^3} \quad (3)$$

The first, second, and third terms on the right hand side of Eq.(2) are expressions for the boundary viscous drag, Darcy frictional drag which is responsible for the porous structure and inertia drag. The term $(\nu u/\beta)$ on the right hand side of Eq. (3) is the modification of the momentum equation to represent the elastic and non Newtonian contribution in the total resistance, where β is another drag parameter that depends upon the porous media's geometry (d and ϵ) as well as the non-Newtonian drag parameter ψ and is derived by El Kady et al. [23] as:

$$\beta = \frac{d^2 \epsilon^3}{\psi (1 - \epsilon)^2} \quad (4)$$

where ψ is the non-Newtonian drag parameter which depends upon the polymer type and concentration and was derived by Rabie et al. [24] as;

$$\psi = N \cdot (C [\mu])^n \quad (5)$$

where C , $[\mu]$ are the mass concentration of the polymer molecules, the intrinsic viscosity and N and n are numerical constants. The values of the parameters $[\mu]$, N and n are given in details in Rabie et al. [24].

The present model using Eqs. (4) and (5) can be used for the flow of Newtonian fluid ($\psi = 0$) as well as drag reducing fluids ($\psi > 0$) in porous media.

The porosity " ϵ " was assumed to vary exponentially from the wall according to the following form:

$$\epsilon = \epsilon_e \left[1 + b \exp(c \cdot [r_0 - r] / d) \right] \quad (6)$$

where ϵ_e is the free stream porosity, and the empirical constants b and c were chosen similar to that used by [17,20] among others

The boundary conditions imposed on the physical system are uniform with respect to the axial coordinate, the computational domain thus comprises of one half of the pipe. At the channel inlet, the fluid has a uniform velocity u_m and uniform temperature T_i . At the outer radius there is no slip condition with either uniform heat flux q_w or constant wall temperature T_w , i.e. the following boundary conditions are applied:

$$T = T_i, u = u_m \text{ at the inlet section where } x = x_i.$$

$$u = 0 \text{ at } r = r_o, du/dr = 0 \text{ at } r = 0$$

$$q = q_w \text{ for constant heat flux, or}$$

$$T = T_w \text{ for constant wall temperature at } r = r_o$$

In order to nondimensionalize the governing equations (1) and (2), the following scalings are used:

$$U = u/(v/r_o), R = r/r_o, D = d/r_o, X = (x - x_i)/(r_o \cdot Pr) \text{ and } \theta = (T - T_i)/\theta_c$$

where θ_c is the characteristic temperature

$$= (q_w \cdot r_o / k_e) \text{ for constant wall heat flux and}$$

$$= (T_w - T_i) \text{ for constant wall temperature,}$$

k_e is the effective thermal conductivity, and

Pr is the Prandtl number $= \nu/\alpha_e$

The energy and momentum Eqs. (1) and (2) can be transformed to nondimensional form as:

$$U \partial \theta / \partial X = 1/R \cdot [\partial / \partial R (R \cdot \partial \theta / \partial R)] \quad (7)$$

$$U + C_1 U^2 = \Gamma \cdot B + (\Gamma / R) \cdot [\partial / \partial R (R \partial U / \partial R)] \quad (8)$$

where, $C_1 = 1.75 D / [(\psi + 175)(1 - \epsilon)]$,

$$\Gamma = D^2 \epsilon^3 / [(\psi + 175)(1 - \epsilon)^2] \text{ and,}$$

$$B \text{ is a nondimensional pressure gradient } = -dP/dx \cdot [r_o^3 / \rho \nu^2]$$

The important heat transfer characteristics in a channel flow are indicated by the Nusselt number and the thermal entrance length which characterize the thermal layer development.

Nusselt number at the wall can be derived in the dimensionless form as [20]:

$$Nu = \partial T / \partial r |_{r=r_o} \cdot 2 [r_o / (T_w - T_m)] \quad (9)$$

where the subscript w refers to the wall of the duct, T_m is the mean fluid temperature defined in the nomenclature in a manner similar to that for classical fluid duct flows.

The thermal entrance length X_f was defined as the distance between the entrance of the pipe and the point at which the mixed mean fluid temperature θ_m and the Nusselt number Nu become independent of the X -location, i.e. $\partial \theta_m / \partial X = \partial Nu / \partial X = 0$, and θ_m can be defined as:

$$\theta_m = (T_w - T) / (T_w - T_m)$$

3. Method of Solution

The dimensionless governing equations were solved numerically utilizing a finite difference scheme. The diffusion terms in the momentum and energy equations were approximated by a central difference scheme. The Forschheimer nonlinear term is linearized by guessing initial valued of the velocity field at all the grid points, and the nonlinear term was written as the product of the unknown velocity and the guessed velocity. The dimensionless radius was discretized into 181 unequally spaced increments to get an accurate resolution of the important near-wall region which is used to obtain the momentum equation finite difference form. A very fine grid size in the X direction near the channel inlet and coarser downstream is used. The grid size at the inlet is 0.0001 and increases gradually in the downstream direction. This is done to capture the steep changes in the temperature field near the entrance. Finite difference equation derived from the momentum Eq. (8) constitutes a set of simultaneous linear equations of 182 dimensions and were solved by Gaussian elimination to yield the velocity field. Utilizing the velocity distribution thus obtained, and after finite differencing the energy equation (7) using an implicit method, a system of tridiagonal algebraic equations for the nodal temperature at any given X position is obtained. The TDMA (Thomas algorithm) is used to solve the system of equations beginning at $X=0$ and marching downstream. Once the temperature profile at each X position is known the local Nusselt number is determined from Eq. (9). When the local gradient of Nusselt number and mixed mean fluid temperature θ_m with respect to X is less than 0.0001, a thermally fully developed flow is assumed and the entrance length is obtained.

4. Results and Discussion

4.1 Model Validation

To examine the adequacy of the present heat transfer model, to the knowledge of the authors there are no heat transfer studies considering non-Newtonian fluid flow through saturated cylindrical porous media either experimentally or theoretically, therefore, the governing equations were solved under conditions corresponding to those in Poulidakos and Renken [20] during their work in the developing region for forced convection of the Newtonian fluid flow in cylindrical porous media. The comparison of the calculated Nu_f with that of Poulidakos and Renken [20] are given in table 1 for sphere diameters $d = 3$ and 5 mm, $\psi = 0$, $0.05 \leq D \leq 0.15$ and $10^4 \leq B \leq 10^6$. The agreement is satisfactory, since the difference is, except in two cases, less than 2%, confirming the adequacy of the presented heat transfer model.

4.2 Thermal Entrance Length

In order to establish the relative influence of the non-Newtonian effects of the drag reducing fluids on the forced convective heat transfer in porous material filled pipes,

numerical results have been obtained for $d=3.2$ mm, $D=0.32$, $0 \leq \psi \leq 5000$, $0.5 \leq Re \leq 10^5$ and B up to 10^{10} for both the two boundary conditions, namely CWT and UHF.

Table 1 Comparison of the calculated Nu_f with that of Poulidakos and Renken [20]

d	D	B	this work Nu_f	Poulidakos and Renken [20] Nu_f	% difference in Nu_f
3	0.1	10^4	7.366	7.35	0.218
3	0.1	2.5×10^4	7.407	7.35	0.776
3	0.1	5×10^4	7.377	7.35	0.367
3	0.1	7.5×10^4	7.416	7.35	0.898
3	0.1	10^5	7.410	7.35	0.816
3	0.1	2.5×10^5	7.369	7.35	0.258
3	0.1	5×10^5	7.385	7.35	0.476
3	0.1	7.5×10^5	7.332	7.35	0.245
3	0.1	10^6	7.360	7.35	0.136
3	0.05	10^5	6.695	7.00	4.5
3	0.075	10^5	7.090	7.20	1.55
3	0.125	10^5	7.663	7.51	1.99
3	0.15	10^5	7.827	7.66	2.13
5	0.1	10^4	7.695	7.6	1.25
5	0.1	2.5×10^4	7.703	7.6	1.36
5	0.1	5×10^4	7.730	7.6	1.71
5	0.1	7.5×10^4	7.681	7.6	1.07
5	0.1	10^5	7.685	7.6	1.12
5	0.1	2.5×10^5	7.702	7.6	1.34
5	0.1	5×10^5	7.664	7.6	0.84
5	0.1	7.5×10^5	7.666	7.6	0.87
5	0.1	10^6	7.649	7.6	0.64

Figure 2 shows the dependence of the thermal entrance length on ψ for $0 \leq \psi \leq 5000$ and $10^5 \leq B \leq 10^8$ for both CWT and UHF. The entrance length for $B = \text{const.}$ is exactly the same for both the two boundary conditions CWT and UHF which validates the presented model. With the increase of ψ the entrance length decreases because of the increase of Re . Table 2 shows the decrease in the thermal entrance length due to the increase of ψ for $B = 10^6$. An increase of ψ to 250 which corresponds for an example to an addition of 0.25 wppm of polyacrylamide causes reduction of the entrance length from 17 to 9.67. This means a reduction of 43.1%, while an increase of ψ to 500 which means $C=1$ wppm of polyacrylamide causes a decrease of the entrance length of 61.2% and an increase of ψ from 3000 to 5000 causes a reduction in X_f of 2.2%. Figure 2 and table 2 show that the entrance length decreases with the increase of ψ and its behavior takes 3 forms: i.e. sudden decrease of X_f for $\psi \leq 500$, transient decrease for $500 \leq \psi \leq 3000$ and nearly constant (very small effect of ψ) for $\psi \geq 3000$.

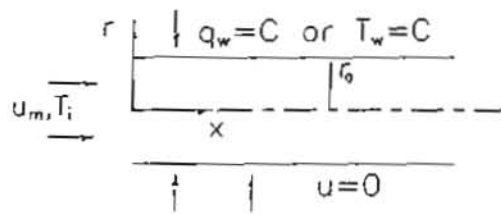


Fig. 1 Physical model, Coordinate system and boundaries

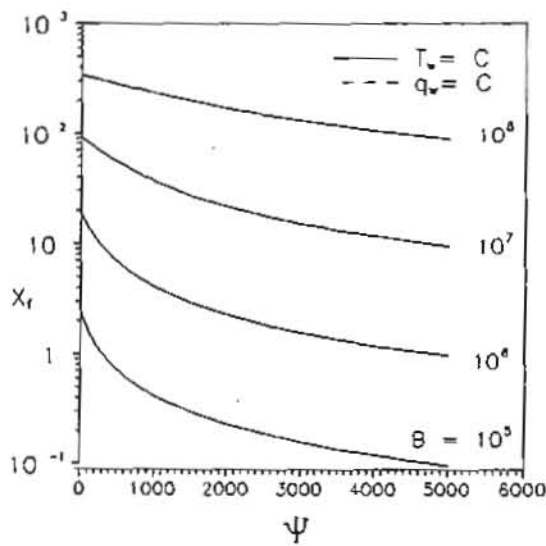


Fig. 2 The thermal entrance length X_f as a function of ψ and B for $D = 0.32$, CWT and UHF

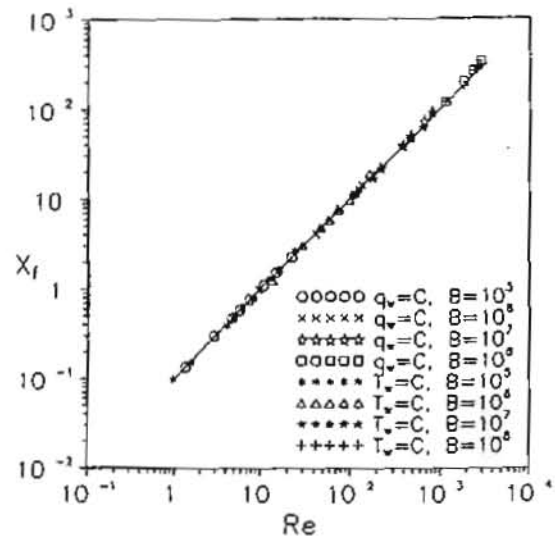


Fig. 3 The thermal entrance length X_f as a function of Reynolds number Re for $D = 0.32$, CWT and UHF

Table 2 The influence of ψ on the thermal entrance length (at $B = 10^6$), Nu (at $Re = 50, X=0.01$) and fully developed Nusselt number Nu_f (at $Re = 100$)

ψ	C	$B=10^6$		Re= 50, X=0.01				Re=100			
				$q_w=c$		$T_w=c$		$q_w=c$		$T_w=c$	
		X_f	%	Nu	%	Nu	%	Nu_f	%	Nu_f	%
0	0	17	100	86.17	100	68.21	100	12.07	100	8.07	100
250	.25	9.67	56.9	97.38	113	76.31	111.9	13.3	110.2	8.67	107.4
500	1	6.6	38.8	103.43	120	80.47	118	13.88	115	8.93	110.7
1000	4	4.1	24.1	111.03	128.85	85.46	125.3	14.49	120	9.19	113.9
2000	17	2.2	12.9	119.12	138.24	90.33	132.43	15.02	124.4	9.4	116.5
3000	37	1.33	7.82	124.02	143.9	93.07	136.47	15.3	126.8	9.52	118
4000	70	1.1	6.47	127.6	148.08	94.97	139.23	15.46	128.1	9.57	118.6
5000	100	0.95	5.59	130.13	151.02	96.19	141.02	15.57	129	9.62	119.2

Figure 3 pertains a heat transfer result of engineering interest, namely, the dependence of the thermal entrance length X_f on Reynolds number. All the cases presented on Fig. 2 which present the two boundary conditions for $0 \leq \psi \leq 5000$, $10^5 \leq B \leq 10^8$ and $0.5 \leq Re \leq 3 \times 10^3$, are represented in Fig. 3. All these points collapse on one curve giving the linear relation in the logarithmic graph of X and Re as follows:

$$X_f = 0.1 Re \quad (10)$$

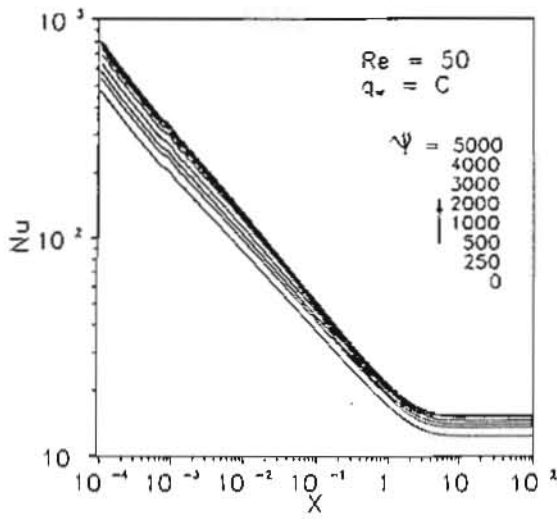
Defining Graetz number based on the pipe diameter $Gz = (D/x).Pr.Re$, this relation will be transformed to give the reciprocal of Graetz No. at the entrance length x_f for the flow as follows:

$$Gz^{-1} = 0.05 \quad (11)$$

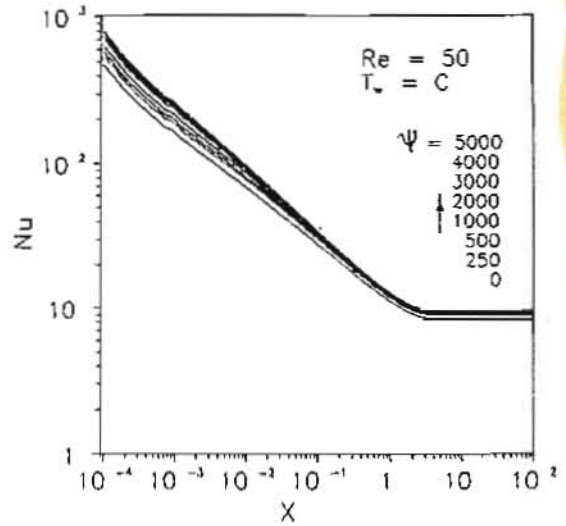
Equations 10 and 11 mean that the fully developed conditions are reached for $[(\infty D)/Re.Pr] = 0.05$, which is also obtained by El Kady [18] for the Newtonian fluid flow in the porous media and can be obtained from the results of Kays et al [26] for the pure laminar fluid flow. i.e. this relation is also valid for the non-Newtonian drag reducing fluid flow in the porous media.

4.3 Development of Heat Transfer

The development of heat transfer of drag reducing fluid flow in a porous medium is investigated by plotting local values of Nusselt number as a function of X according to Eq. (9). The results for the thermal entry region and the fully developed region are shown in Figs. 4 to 7 for different values of Reynolds number and pressure gradients B for both the two boundary conditions CWT and UHF. As it was expected, Nu decreases with the increase of X in the entrance region to their asymptotic fully developed value. Because the thermal boundary layer thickness is zero at the tube entrance, the convection coefficient is extremely large and the Nusselt number are in principle, infinite at $X=0$. However, Nu decreases rapidly as the thermal boundary layer develops, until the constant value associated with the fully developed conditions is reached.

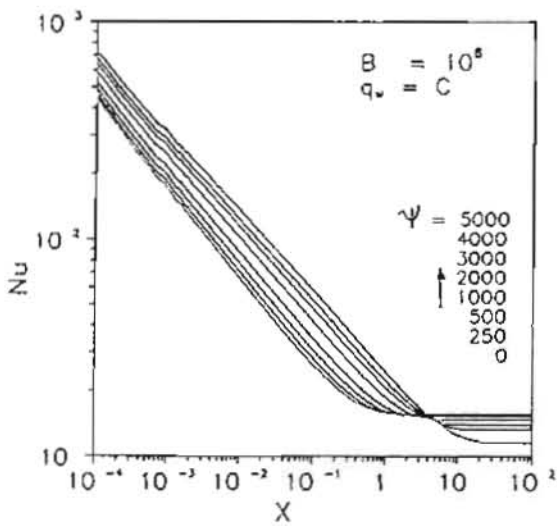


a

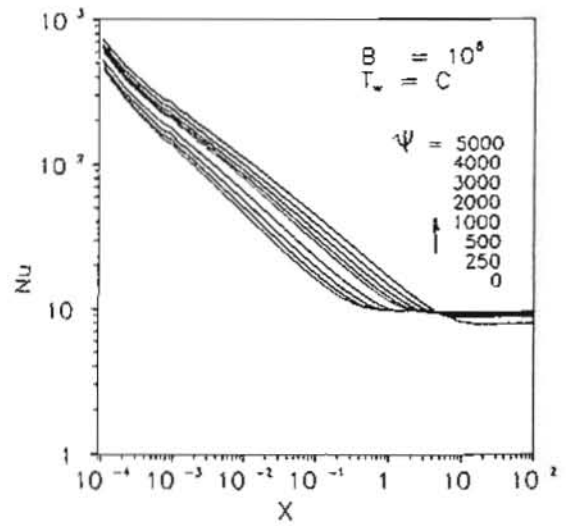


b

Fig. 4a,b Effect of drag parameter ψ on the local Nu for $Re = 50, D = 0.32$
a: UHF; b: CWT



a



b

Fig. 5a,b Effect of drag parameter ψ on the local Nu for $B = 10^6, D = 0.32$
a: UHF; b: CWT

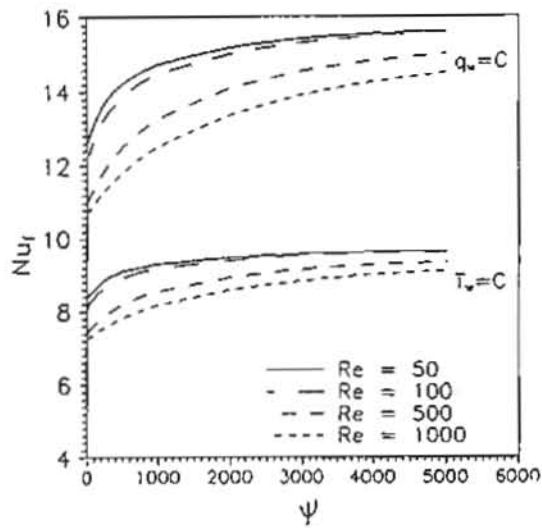


Fig. 6 The fully developed Nu_f as a function of ψ and Reynolds number Re for $D = 0.32$, CWT and UHF

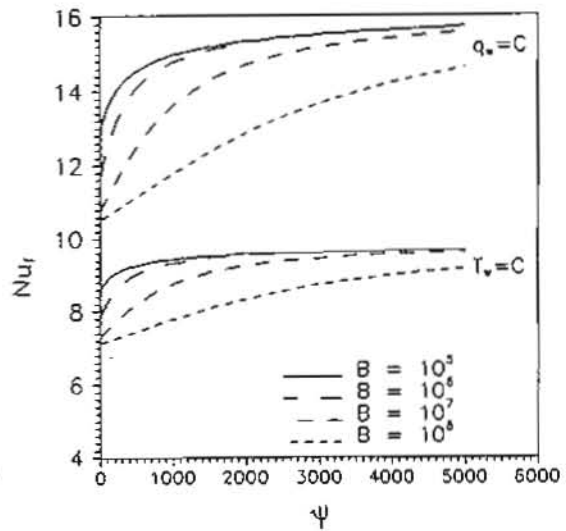
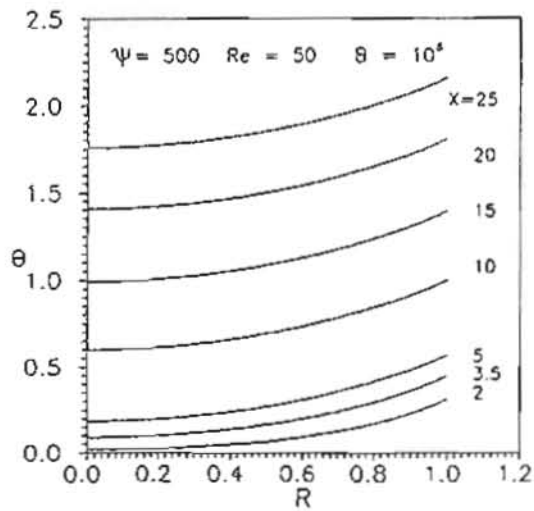
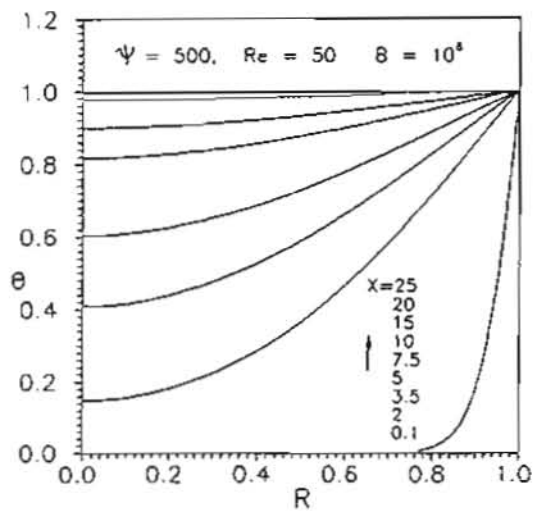


Fig. 7 The fully developed Nu_f as a function of ψ and the pressure drop B for $D = 0.32$, CWT and UHF



a



b

Fig. 8a,b Temperature distribution across the pipe half width at several X locations for $\psi = 500$, $Re = 50$, $B = 10^6$ and $D = 0.32$. a: UHF; b: CWT

Figure 4 represents the Nusselt number variation in the developing and fully developed regions for different values of ψ ranging from 0 to 5000 and $Re = 50$. The cases (a) and (b) are for UHF and CWT respectively. Both Fig. 4 and table 2 show that the increase of ψ to 500 causes an increase of Nu at $X=0.01$ of about 18% for the case of CWT and about 20% for UHF, while the increase of ψ from 3000 to 5000 increases the entrance length by only 3.4% for CWT and about 4.9% for UHF. It is observed that the local Nusselt number in the entire developing and developed regions increases with the increase of ψ until $\psi=3000$. For constant Re , increasing ψ increases B and increases the channeling effect [23], which in turn yields to higher values of Nusselt number throughout the developing and fully developed regions. However, for $\psi \geq 3000$ no significant influence for ψ appears.

Figure 5 represents the Nusselt number variation in the thermal entry and the fully developed regions for different values of ψ at $B=10^6$. The cases (a) and (b) are for UHF and CWT respectively. For $B=const.$ increasing ψ decreases Re which means slower flow and increases the channeling effect [23] yielding to lower values of Nu throughout the thermal entry region and higher values of Nu_f in the fully developed region.

The fully developed values of Nu_f are represented in Figs. 6 and 7 for both the boundary conditions, for $0 \leq \psi \leq 5000$ and $Re=50, 100, 500$ and 1000 in Fig. 6 and for $B=10^5, 10^6, 10^7$ and 10^8 in Fig. 7. Table 2 shows for the case of UHF that the increase of ψ to 500 which corresponds for an example to 1 wppm of polyacrylamide causes an increase of Nu_f of about 15%, while the increase of ψ from 500 to 1000 ($C=1$ to 4 wppm) gives an increase of Nu_f of about 4.4% and the increase from 3000 to 5000 ($C=37-100$ wppm) causes an increase of Nu_f of only 1.7%. Figures 6 and 7 and Table 2 observe that in all the represented cases three types of behavior for Nu_f with the increase of ψ are exhibited, namely, sharp increase in Nu_f for $\psi \leq 500$ due to the sharp decrease of the channeling velocity, transient increase for $500 \leq \psi \leq 3000$ due to the lower rate of the channeling velocity increase and nearly constant for $\psi \geq 3000$ for the very low rate of channeling velocity increase [23]. For $\psi=const.$ Nu_f decreases with the increase of either Re or B . Nu_f for the case of CWT is as expected less than it at the UHF case.

4.4 Temperature Variation

Figure 8 shows the nondimensional temperature distribution across the pipe half width at several downstream locations $X = 0.1, 2, 3.5, 5, 7.5, 10, 15, 20$ and 25 where the entrance length $X_f = 5$, $\psi = 500$, $Re = 50$ and $B = 10^6$. The cases (a) and (b) are for UHF and CWT respectively. Typical temperature profiles are shown and characterized by a steep gradient at the wall owing to the effects of wall channeling.

Figure 9 presents the variation of the temperature across the pipe half width at a location $X = 5$, $Re=50$ and $0 \leq \psi \leq 5000$ for both cases of UHF and CWT. As presented in table 3, $\Delta\theta$ (the difference between the wall temperature and the core temperature) decreases with the increase of ψ , which means faster propagation of the heating effect of the walls. This is because of the increase of the channeling effects with the increase of ψ for constant Re [23].

Table 3 Dependence of $\Delta\theta$ (the difference between the wall temperature and the core temperature) and $\Delta\theta_m$ on ψ for $Re=50$, $X=X_f=5$.

ψ	C	$T_w=c$		$q_w=c$		$q_w=c$		$T_w=c$	
		$\Delta\theta$	%	$\Delta\theta$	%	$\Delta\theta_m$	%	$\Delta\theta_m$	%
0	0	0.4247	100	0.4004	100	1.7314	100	1.5503	100
500	1	0.3958	93.2	0.382	95.4	1.7764	102.6	1.5851	102.2
1000	4	0.3909	92.0	0.3768	94.1	1.7887	103.1	1.5948	102.9
3000	37	0.3791	89.3	0.3711	92.7	1.8038	104.2	1.6073	103.7
5000	100	0.3763	88.6	0.3691	92.2	1.8087	104.5	1.6113	103.9

Figures 10 and 11 present the temperature variation of across the pipe half width at $X=5, 10$ and 15 , $B=10^6$ and $0 \leq \psi \leq 5000$. Figure 10 shows the case of UHF while Fig. 11 shows the case of CWT. With the increase of ψ Reynolds number decreases sharply but the channeling effect increases [23] and $\Delta\theta$ (the difference between the wall temperature and the core temperature) decreases which means faster propagation of the heating effect of the walls, this is mainly because of the increase of the channeling effects [23].

The influence of the non-Newtonian drag reducing fluids on the mixed mean fluid temperature θ_m is shown in Fig. 12 for $Re=50$ and $X=5$. From the profiles shown, it is evident that the increase of ψ leads to an increase of θ_m near the wall and in the core region for $\psi < 3000$. However, for $\psi \geq 3000$ no remarkable change in the profiles of θ_m which indicates negligible influence after $\psi=3000$. Table 3 presents $\Delta\theta_m$ (the difference of θ_m between the core and the wall) with the change of ψ . $\Delta\theta_m$ increases with the increase of ψ until $\psi=3000$ and no remarkable changes for $\psi > 3000$. Fig. 12 shows also that θ_m near the wall for the UHF is higher than it for the CWT, while it is less in the core region for the UHF than it for the CWT.

5. Conclusions

The effects of the elongational viscosity of the non-Newtonian drag reducing fluids on the forced convection heat transfer parameters such as the thermal entrance length, temperature profiles and heat transfer Nusselt number were studied for CWT and UHF boundary conditions. The present conclusions was obtained:

- For constant B fluids with very low values of the drag parameter ψ can cause high reduction in the entrance length. The entrance length decreases with the increase of non-Newtonian drag parameter ψ and its behavior takes 3 forms, sudden decrease of X_f for $\psi \leq 500$, transient decrease for $500 \leq \psi \leq 3000$ and nearly constant for $\psi \geq 3000$
- X_f increases linearly with Re and gives the same correlation that obtained for the pure fluid flow and Newtonian fluid flow in porous media as:

$$X_f = 0.1 Re, \quad Gz^{-1} = 0.05$$

- Fluids with very low values of the drag parameter ψ cause a high change in the local Nusselt number in the entire developing and developed regions.

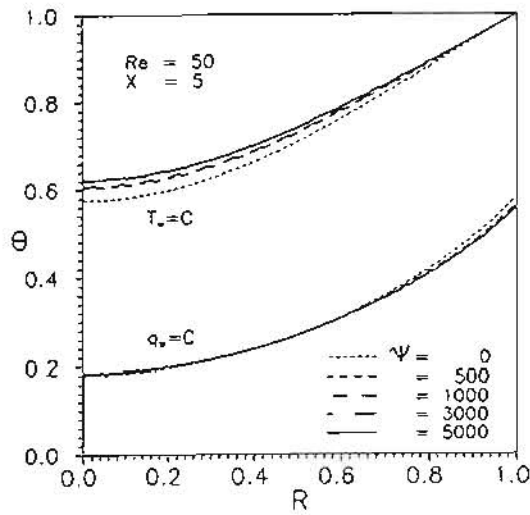


Fig. 9 Temperature variation across the pipe half width for different values of ψ , $Re = 50$, $D = 0.32$ and $X=5$. a: UHF; b: CWT

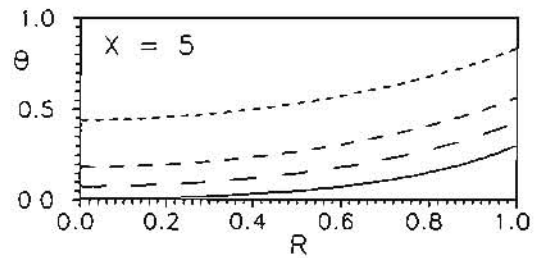
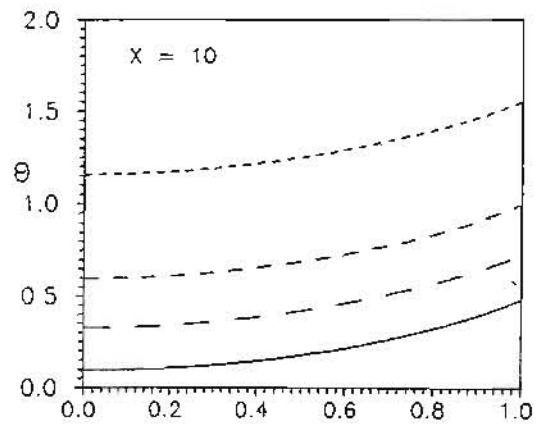
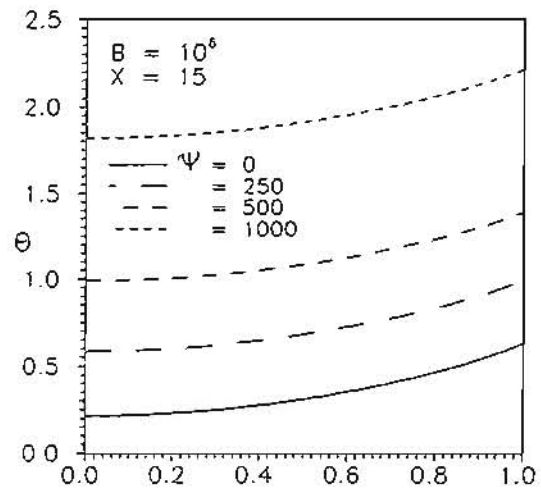


Fig. 10 Temperature variation across the pipe half width at $X=5, 10$ and 15 for different values of ψ , $B=10^6$, $D = 0.32$ and UHF

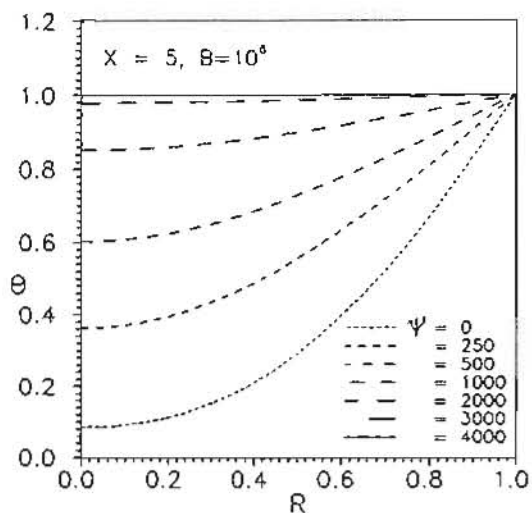
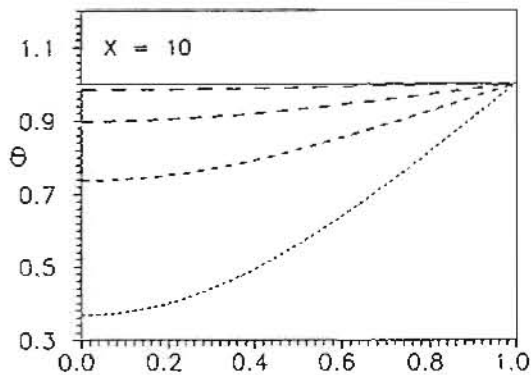
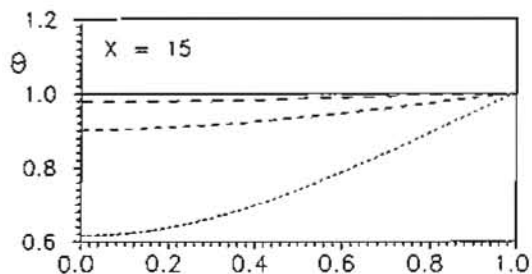


Fig. 11 Temperature variation across the pipe half width at $X=5, 10$ and 15 for different values of $\psi, B = 10^6, D = 0.32$ and CWT

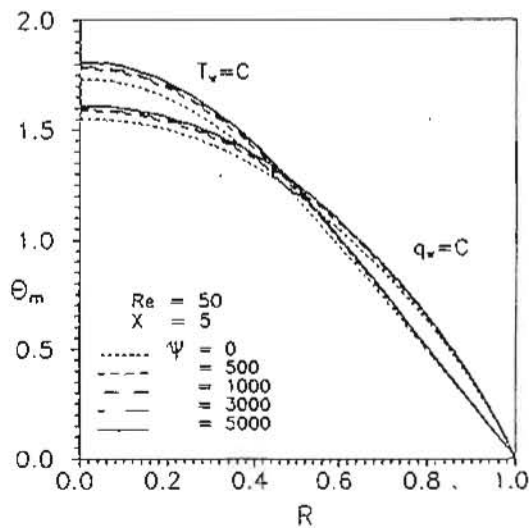


Fig. 12 Influence of drag parameter ψ on the mixed mean temperature θ_m at $X=5$ for $Re = 50, D = 0.32, CWT$ and UHF

- In the developing region, increasing ψ at constant Re increases B which gives higher values of Nu . For constant B , increasing ψ decreases Re which yields to lower values of Nu until $\psi = 3000$. However, for $\psi \geq 3000$ no significant influence for ψ appears.
- In the fully developed region, three types of behavior for Nu_f with the increase of ψ are exhibited, sharp increase for $\psi \leq 500$, transient increase for $500 \leq \psi \leq 3000$ and nearly constant for $\psi \geq 3000$. For $\psi = \text{const}$, Nu_f decreases with the increase of either Re or B .
- With the increase of ψ , $\Delta\theta$ (the difference between the wall temperature and the core temperature) decreases, which means faster propagation of the heating effect of the walls to the core region due to the increase of the channeling effects.
- The increase of ψ leads to an increase of the mixed mean fluid temperature θ_m near the wall and in the core region for $\psi < 3000$. However, for $\psi \geq 3000$ no remarkable change in the profiles of θ_m which indicates negligible influence after $\psi = 3000$. θ_m near the wall for the UHF is higher than it for the CWT, while it is less in the core region for the UHF than it for the CWT.

6. Nomenclature

A	Forschheimer inertia coefficient of the porous medium, equation (2), m^{-1}
b, c	constants, equation (6)
B	nondimensional pressure gradient, equation (8)
C	concentration of the polymer molecules equation (5); in wppm
C_1	dimensionless coefficients, equation (8)
d, D	sphere diameter, m, dimensionless sphere diameter = d/r_0
Gz	Graetz number based on the pipe diameter $Gz = (D/x) \cdot Pr \cdot Re$
k_e	effective thermal conductivity, kW/m K
α, N	numerical constants, equation (5)
Nu	Nusselt number, equation (9)
Nu_f	Nusselt number at the thermal entrance length
P	pressure, Pa
Pr	Prandtl number = ν/α_e
q_w	mean wall heat flux, kW/m ²
r	radial coordinate, m
r_0	pipe radius, m
R	dimensionless radial coordinate
Re	Reynolds number based on the tube diameter = $2 u_m \cdot r_0/\nu$
T	temperature, K
T_i	temperature at the inlet section $x = x_i$, K
T_m	mean temperature, $T_m = \left(\int_0^{r_0} \rho u T r dr \right) / \left[\int_0^{r_0} \rho u r dr \right]$
T_w	wall temperature, K
u	field velocities in the x direction, m/s
u_m	local averaged fluid velocity including the solid and fluid regions, m/s
U	non-dimensional field velocity in the X direction
x	axial coordinate

x_i	channel inlet axial distance
X	dimensionless distances in the x axis = $(x - x_i) / (r_0 \cdot Pr)$
X_f	thermal entry length
α_e	effective thermal diffusivity of the porous medium, m^2/s
β	non-Newtonian drag parameter, equation (2).
γ	permeability of the porous layer, equation (2), m^2
Γ	dimensionless coefficients, equation (8)
ψ	drag parameter, equation (4).
ε	porosity of the porous medium
ε_e	free-stream porosity
θ	non-dimensional temperature = $(T - T_i) / \theta_c$
θ_c	characteristic temperature
θ_m	invariant mixed mean temperature = $(T_w - T) / (T_w - T_m)$
$[\mu]$	intrinsic viscosity
ν	kinematic viscosity of the fluid, m^2/s
ρ	fluid density, kg/m^3

7. References

1. Shenoy, A. V., "Handbook of Heat Mass Transfer," Vol. 1, Gulf, Houston, TX, Chapter 5, p. 183, 1986.
2. Shenoy, A. V., "Encyclopedia of Fluid Mechanics," Vol. 7, Gulf, Houston, TX, Chapter 10, p. 287, 1988.
3. Chen, H. T. and Chen, C. K., "Free Convection Flow of Non-Newtonian Fluid Along a Vertical Plate Embedded in a Porous Medium," ASME J. of Heat Transfer, Vol. 110, pp. 257-260, 1988.
4. Wang, C. and Tu, C., "Boundary-layer Flow and Heat Transfer on Non-Newtonian Fluids in Porous Media," Int. J. Heat Fluid Flow, Vol. 10, pp. 160-165, 1989.
5. Pascal, H. and Pascal, P., "Nonlinear Effects of Non-Newtonian Fluids on Natural Convection in a Porous Medium," Physica D, Vol. 40, pp. 393-402, 1989.
6. Pascal, H., "Non-isothermal Flow of Non-Newtonian Fluids Through a Porous Medium," Int. J. Heat Mass Transfer, Vol. 33, pp. 1937-1944, 1990.
7. Wang, C., Tu, C. and Zhang, X., "Mixed Convection of Non-Newtonian Fluids from a Vertical Plate Embedded in a Porous Medium," Acta Mechanica Sinica, Vol. 6, pp. 214-220, 1990.
8. Nakayama, A. and Koyama, H., "Buoyancy-induced Flow of Non-Newtonian Fluids over a Non-isothermal Body of Arbitrary Shape in a Fluid-saturated Porous Medium," App. Sci. Res. Vol. 48, pp. 55-70, 1991.
9. Nakayama, A. and Shenoy, A. V., "Combined Forced and Free Convection Heat Transfer in Non-Newtonian Fluid Saturated Porous Medium," App. Sci. Res. Vol. 49, 1992.
10. Amiri, B., Vasseur, P., and Bilgen, E., "Natural Convection of Non-Newtonian Fluids in a Horizontal Porous Layer," Wärme und Stoffübertragung, 29, pp. 185-193, 1994.

11. Yang, Y. T. and Wang, S. J., "Free Convection Heat Transfer of Non-Newtonian Fluids Over Axisymmetric and Two-dimensional Bodies of Arbitrary Shape Embedded in a Fluid Saturated Porous Medium," *Int. J. Heat Mass Transfer*, Vol. 39, pp. 203-210, 1996.
12. Shenoy, A. V., "Darcy-Forschheimer Natural, Forced and Mixed Convection Heat Transfer in Non-Newtonian Power-law Fluids-Saturated Porous Media," *Transport in Porous Media*, Vol. 7, 1992.
13. Nakayama, A. and Shenoy, A. V., "A Unified Similarity Transformation for Darcy and Non-Darcy Forced-, Free- and Mixed Convection Heat Transfer in Non-Newtonian Inelastic Fluid Saturated Porous Media," *The Chemical Eng. Journal*, Vol. 50, pp. 33-45, 1992.
14. Nakayama, A. and Shenoy, A. V., "Non-Darcy Forced Convective Heat Transfer in a Channel Embedded In a Non-Newtonian Inelastic Fluid Saturated Porous Medium," *The Canadian J. of Chemical Engineering*, Vol. 71, pp. 168-173, 1993.
15. Vafsa, K., and Kim, S. J., "On the Limitations of the Brinkman-Forschheimer-Extended Darcy Equation," *Int. J. Heat and Fluid Flow*, Vol. 16, pp. 11-15, 1995.
16. Hayes, R.E., "Forced Convection Heat Transfer at the Boundary Layer of a Packed Bed," *Transport in Porous Media*, Vol. 5, pp. 231-230, 1990
17. El Kady, M., "Forced Convection Heat Transfer and Flow in an Annular Porous Medium in the Non-Darcian Effects," *Mansoura Engineering Journal*, Vol. 19, No. 3, pp. M9- M26, September 1994.
18. Kamiuto, K. and Saitoh, S., "Fully Developed Forced-Convection Heat Transfer in Cylindrical Packed Beds with Constant Wall Temperatures," *JSME Int. J., Series B*, Vol. 37, No. 3, pp. 554-559, 1994.
19. El Kady, M.S., Tolba, M. A. and Rabie, L. H., "Flow in a Circular Pipe Filled With Porous Medium in the non-Darcian Effects," To be Published.
20. Poulidakos, D., and Renken, K., "Forced Convection in a Channel Filled with Porous Medium, Including the Effects of Flow Inertia, Variable Porosity, and Brinkman Friction," *ASME J. of Heat Transfer*, Vol. 109, pp. 880-888, 1987.
21. Nakayama, A., Kokudai, T. and Koyama, H., "Non-Darcian Boundary Layer Flow and Forced Convective Heat Transfer over a Flat Plate in a Fluid-Saturated Porous Medium," *ASME. J. Heat Transfer*, Vol. 112, pp. 157-162, 1990
22. Chea, C. H., Chen, T. S. and Chen, C. K., "Non-Darcy Mixed Convection Along Nonisothermal Vertical Surfaces in Porous Media," *Int. J. Heat Mass Transfer*, Vol. 39, pp. 1157-1163, 1996.
23. El Kady, M.S., Tolba, M. A. and Rabie, L. H., "Non-Newtonian Drag Reducing Fluid Flow in a Circular Pipe Filled With Porous Medium in the non-Darcian Effects," *Mansoura Engineering Journal (MEJ)*, Vol. 21, No. 3, pp. M9- M26, Sep. 1996
24. Rabie, L. H., Arid, F. F., and Shalaby, M. A., "Flow of Dilute Polymer Solutions in Porous Media" *Mansoura Engineering Journal*, Vol. 11, No. 2, pp. M85-M95, December 1986.
25. Ergun, S., "Fluid Flow Through Packed Columns," *Chemical Engineering Progress*, Vol. 48, pp. 89-94, 1952.
26. Kays, W. M., and Crawford, M. E. "Convective heat and mass transfer" Mc Graw Hill, New York, 1980.